



Brookhaven
National Laboratory

BNL-104745-2014-TECH

AGS/AD/Tech Note No. 329;BNL-104745-2014-IR

AGS INJECTION STUDIES WITH THE FAST CHOPPER

M. J. Brennan

September 1989

Collider Accelerator Department
Brookhaven National Laboratory

U.S. Department of Energy

USDOE Office of Science (SC)

Notice: This technical note has been authored by employees of Brookhaven Science Associates, LLC under Contract No. DE-AC02-76CH00016 with the U.S. Department of Energy. The publisher by accepting the technical note for publication acknowledges that the United States Government retains a non-exclusive, paid-up, irrevocable, world-wide license to publish or reproduce the published form of this technical note, or allow others to do so, for United States Government purposes.

DISCLAIMER

This report was prepared as an account of work sponsored by an agency of the United States Government. Neither the United States Government nor any agency thereof, nor any of their employees, nor any of their contractors, subcontractors, or their employees, makes any warranty, express or implied, or assumes any legal liability or responsibility for the accuracy, completeness, or any third party's use or the results of such use of any information, apparatus, product, or process disclosed, or represents that its use would not infringe privately owned rights. Reference herein to any specific commercial product, process, or service by trade name, trademark, manufacturer, or otherwise, does not necessarily constitute or imply its endorsement, recommendation, or favoring by the United States Government or any agency thereof or its contractors or subcontractors. The views and opinions of authors expressed herein do not necessarily state or reflect those of the United States Government or any agency thereof.

Accelerator Division
Alternating Gradient Synchrotron Department
BROOKHAVEN NATIONAL LABORATORY
Upton, New York 11973

Accelerator Division
Technical Note

AGS/AD/Tech. Note No. 329

AGS INJECTION STUDIES WITH THE FAST CHOPPER

J.M. Brennan, L. Ahrens, and J. Alessi

September 12, 1989

Introduction

Injection of fast chopped beam into the AGS was studied in several runs spaced throughout the SEB running period (March 7th, March 15th, April 13th, April 21st, May 3rd, May 15th, and May 24, 1989). The experiments ranged from checkout and adjustment of the fast chopping equipment to analysis of transverse effects at injection, and culminated in the execution of an injection strategy that gave negligible capture losses at low intensity (3×10^{12} ppp) and low losses at a relatively high intensity ($< 10\%$ loss at 13×10^{12} ppp injected). The injected longitudinal phase space emittance is a free parameter with fast chopped injection and in one study, a low emittance beam was created and accelerated to high energy. The emittance of this beam was measured at several points throughout the cycle and is compared to a typical high intensity beam. This report gives the results of these studies and describes the techniques that were used. The material is organized according to topic and not presented chronologically according to studies dates.

For these studies, the injection strategy in transverse or betatron space was to minimize "painting" for simplicity. The result of low losses at relatively high intensity despite this does not appear to agree with intuitive expectations for a space charge dominated machine. Time limitations allowed neither the high intensity machine nor the maximum intensity limit to be explored.

Chopper Performance

The rise and fall times of the H^- current pulse out of the RFQ are less than 10 ns. This is evident in Fig. 1 where the beam current is measured with the fast Faraday cup between the RFQ and the linac. The beam is bunched at 200 MHz at this point, and the microbunches can be seen in the photograph. The fact that only one microbunch occurs during the rise and fall times indicates that the transition times are less than two periods of 200 MHz.

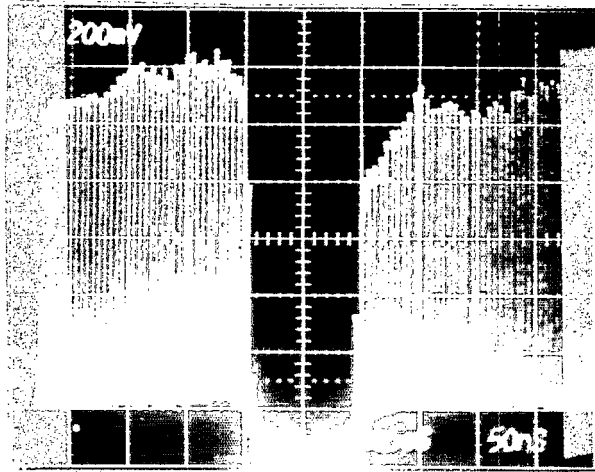
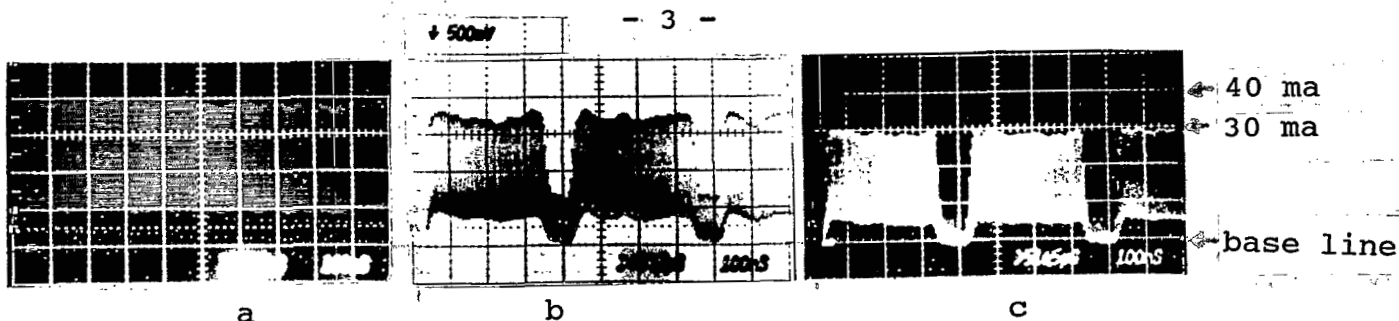


Fig. 1 Beam Current Downstream of RFQ

The fact that the chopper is located between the ion source and the RFQ has the important advantage that the voltage needed to deflect the beam can be obtained from commercially available solid state pulse generators. It has the disadvantage that chopper operation affects the tuning of the beam transport between the source and the RFQ by interacting with the positively charged residual gas which normally neutralizes the space charge of the H^- beam. The significance of this effect can be seen in Figs. 2a to 2c which are measurements with the fast Faraday cup. In Fig. 2a, an unchopped beam is measured. The peak current in the cup is 40 mA and corresponds to a time averaged current out of the linac of 25 mA. When the chopper is turned on, Fig. 2b the peak current, is reduced to 35 mA. Furthermore, the chopping is not very effective. The peak current is only reduced by about 65%. In Fig. 2c the line between the ion source and the RFQ has been retuned so that the chopping is good, but at the cost of an additional loss of peak intensity down to 30 mA. This trade-off between good chopping and high intensity is a characteristic of the chopper. Moreover, as the length of the beam pulse is made



a) unchopped b) partially chopped c) cleanly chopped

Fig. 2 Beam Current vs Chopping Efficiency

shorter, the peak intensity goes down further, reaching a minimum of about 20 mA at around 100 ns as seen in Figs. 3a and 3b. This happens because the voltage is on when the beam is off and the mobility of the positive ions is such that in about 300 ns they are completely swept out.

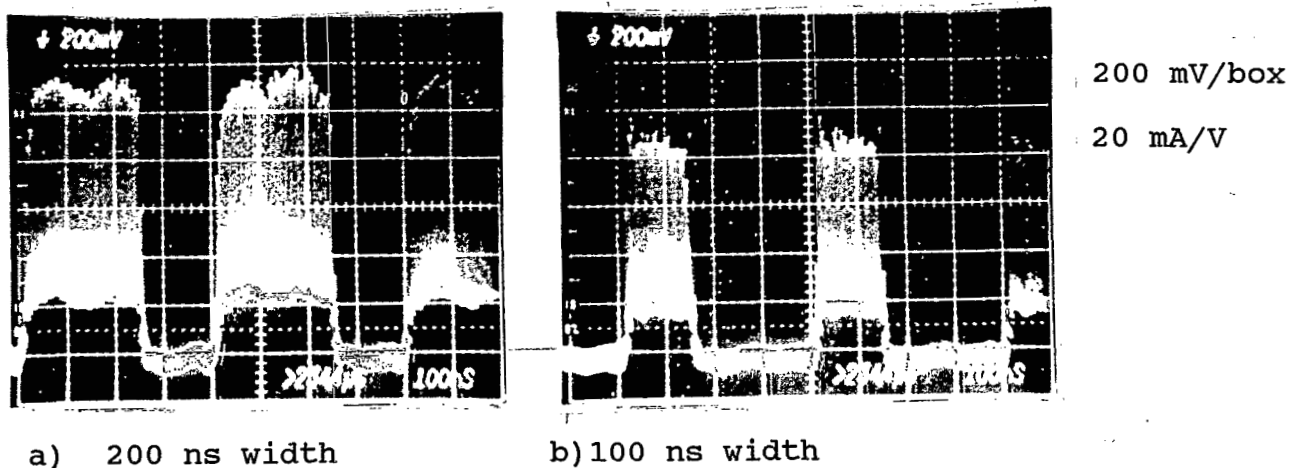


Fig. 3 Beam Current vs Pulse Width

We made three attempts to improve this situation with no success. First, we arranged that the chopper voltage was not turned on until fast chopping actually began and let the chopper at 750 keV "size" the beam. Second, we introduced a partial pressure of about 5×10^{-6} Torr of Xe gas into the chopper box. Xe is easier to ionize than O_2 or N_2 and being heavier, is less mobile. In general, Xe made the beam unstable and did not improve the intensity. Third, we installed a pair of grids at the entrance and exit of the plates with bias applied to produce a longitudinal field pointing into the chopper to confine the loss of neutralization to just the vicinity of the chopper plates. We saw no improvement with any combination of bias polarity.

Linac Beam Measurements

The energy of the linac beam is a critical parameter for injection. The bucket into which we inject is of order 1 MeV in height. We need to arrange the center of the bucket to be at the beam energy to within a small fraction of the bucket height.

This is done by the proper choice of the rf frequency at injection. A precision of one part in 10^4 is achieved by injecting one bunch (typical width of 100 ns) and observing the signal from the F20 wall current monitor as the bunch spirals for 100 turns. By using the LeCroy 9400 digital oscilloscope, we record a 500 microsecond record with 20 ns per sampled point. Figure 4 is a typical measurement. The upper trace is the full record of 103 turns and the lower two traces are expanded views of turns one and 101. The interval between them is obtained by placing the markers at the centers of the pulses. This can be done to ± 20 ns for each pulse and the total interval being 482.06 microseconds implies a precision of 1 part in 17×10^3 .

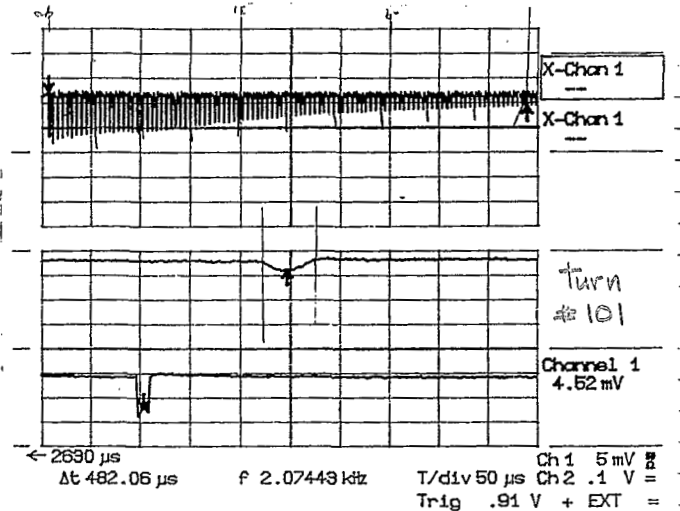


Fig. 4 Single Bunch (Wall Monitor) Observed Over Many Turns

This amounts to a time of flight measurement of the beam speed over a flight path of $101 \times (2 \pi \times 128.457 \text{ meters}) = 81.51903 \text{ km} \approx (50 \text{ miles})$. The change of the effective radius during spiraling due to the rising magnetic field (0.45 T/s) is a small effect because of momentum compaction, and has been neglected. The result is also insensitive to the value taken for the AGS radius. Varying this by 2.5 cm (a large variation) changes the determined kinetic energy by 0.1 MeV. The linac beam energy was measured at the beginning of each run. Table I shows the results. (We quote here the energy of the H^+ beam since it is the

$$\frac{\Delta T}{T} = (1 + \gamma^{-1}) \left(\frac{\Delta t}{t_{db}} \right) \eta^{-1}$$

where Δt is the growth in pulse width during time interval t_{db} . η is $(1/\gamma^2 - \alpha) = - .66$ where α is the momentum compaction factor. γ is 1.21 at 200 MeV.

Figure 6 shows a debunching result. From this data we deduce that the bunch fullwidth grew from 370 ns to 920 ns in 375 microseconds (the first 200 microseconds are ignored because the pulse width is hard to measure from the photo in that interval). This implies an energy spread of ± 0.40 MeV.

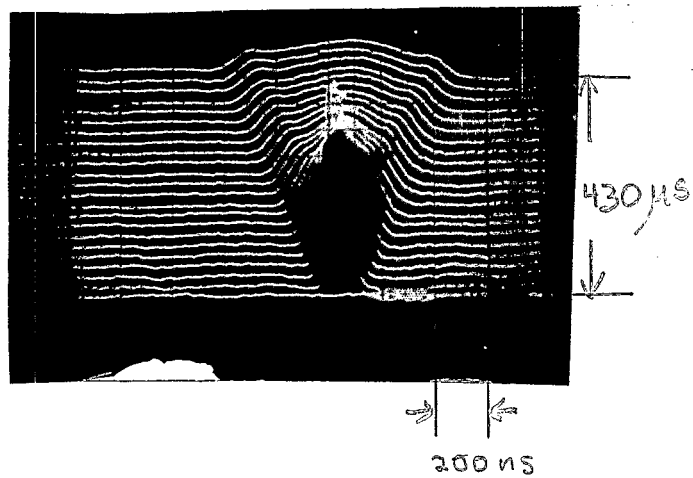


Fig. 6 Wall Monitor Mountain Range of Single Bunch Debunching

Figures 7 and 8 are similar data taken with the LeCroy 9400 digital scope. The widths here (Fig. 7) were measured by using the cursors of the scope and are plotted in Fig. 8. The result here for the spread of the full-width is a slope of 1.84 ns/microseconds, which implies an energy spread of ± 0.51 MeV or $\Delta p/p = \pm 1.3 \times 10^{-3}$.

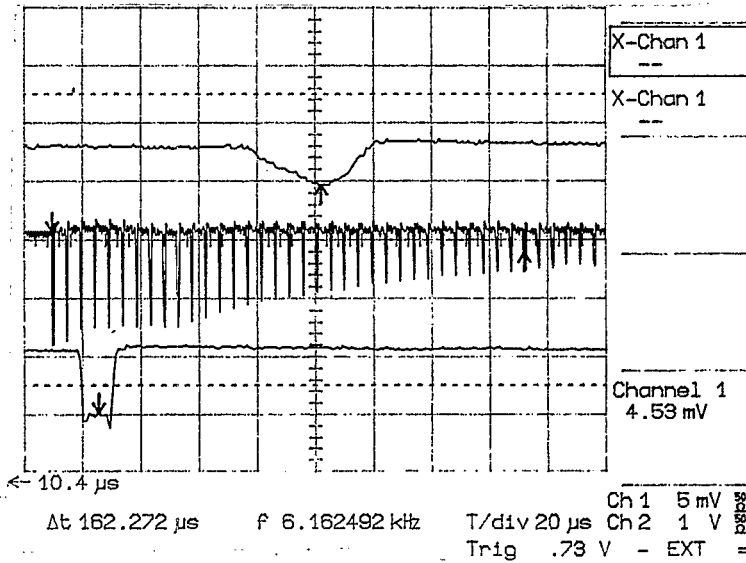


Fig. 7 Debunching on Digital Scope

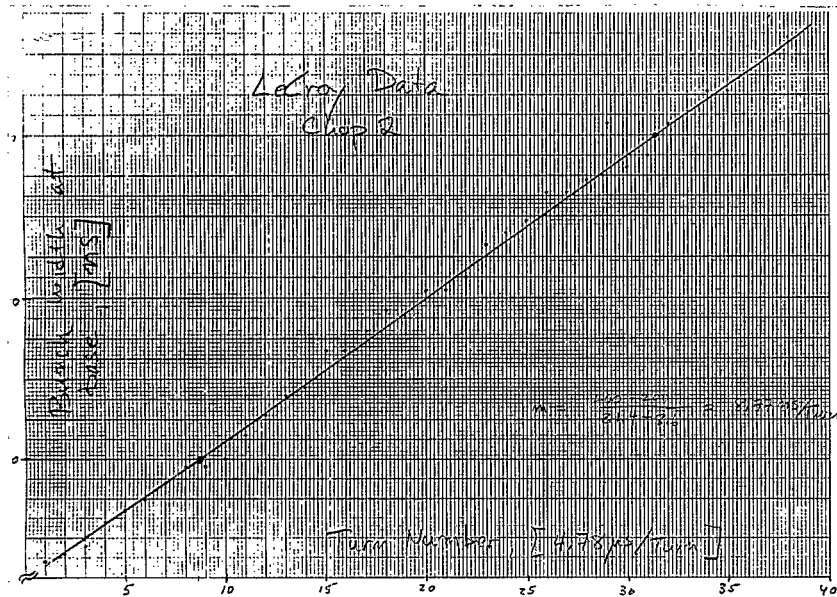


Fig. 8 Debunching: Base Width vs Turn

The second technique is to inject one turn (12 bunches) of short bunches (< 100 ns) into the center of a high voltage rf bucket (250 kV/turn) and observe the beam current on the wall monitor after 1/4 of a synchrotron period. This "bunch rotation" converts the energy distribution (which one cannot see) into a time distribution which is easily measured. Figure 9 (diamond picture) is a mountain range display of the wall current monitor for this situation. By measuring the width when the pulse is the shortest one obtains a measure of the spread in linac beam energy. From Fig. 9, we infer a minimum width of 25 ns, or ± 11.5

degrees of phase. By tracing the trajectory of a point starting on the time axis at 11.5 degrees for 1/4 of a synchrotron period in a bucket corresponding to 204 kV/turn from synchrotron frequency, (see below) we come to a point at 0.096 of the bucket height, 2.4 MeV. This implies a linac energy spread of ± 0.24 MeV.

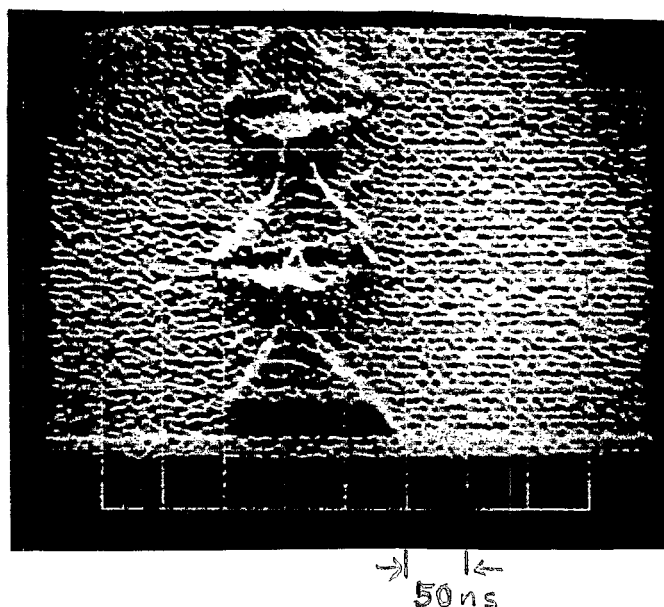


Fig. 9 Wall Monitor Mountain Range Display of Injected Bunch Tumbling in Longitudinal Phase Space

The factor of two difference between the results from the two techniques is presumably due to the fact that the two techniques are sensitive to different aspects of the energy distribution. The first technique really measures all the beam and includes the tails of the distribution, whereas the second technique is more subjective and emphasizes the central peak of the distribution.

(For the "one that got away" column, we remark that it would have been easy doing the bunch rotation experiment to obtain the detailed shape of the distribution. One only needs to record the wall current monitor signal with high resolution on the turn for which it has minimum width. This is straight forward using the fast scope TEK2467 or TEK7104 and the digitizing camera, as was done in the VHF cavity studies, see Studies Note #252. Joseph Kats has simulated this experiment with his tracking code for a calculated linac energy distribution. The calculation is shown in Figure 10.)

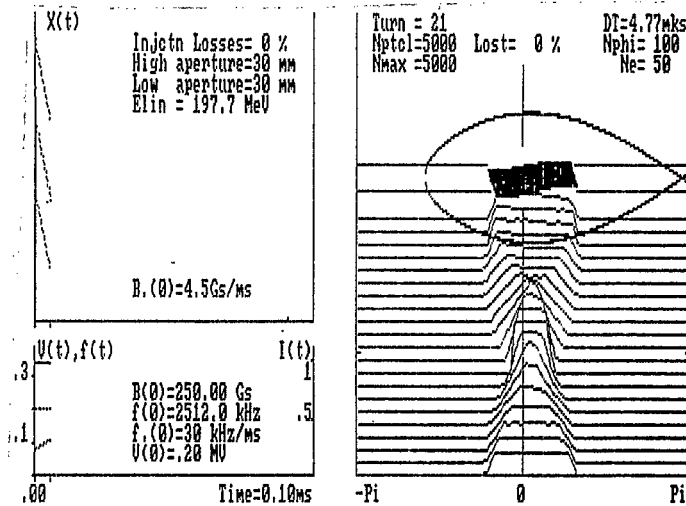


Fig. 10 Computer Simulation of Injected Bunch Tumbling in Bucket

Measurements of AGS Total RF Voltage

The frequency of small amplitude synchrotron oscillations is an unambiguous indicator of the total effective rf voltage per turn. By injecting a short bunch and observing the synchrotron motion we have a clean, model independent, determination of the total rf voltage which does not rely on any direct high-rf-voltage measurements (always a challenge). The error in this measurement is given solely by ones ability to extract the frequency of synchrotron oscillations from data such as Fig. 11. The plot is from the LeCroy 9400 oscilloscope with the F20 wall current monitor as input. The detector gives a negative signal for a positive beam current. The structure is caused by bunch-shape oscillations (or quadrupole mode oscillations) as the injected bunch tumbles in phase space. This is the same type of data as Fig. 9 but viewed at a slow sweep speed. For this case, we obtain a synchrotron frequency of 5.9 ± 0.05 kHz. Even though this is a moving bucket, ϕ_S (the synchronous phase) is only about 8 degrees so that $\cos(\phi_S) = 0.99$. This implies a total rf voltage of 230 ± 4 kV/turn.

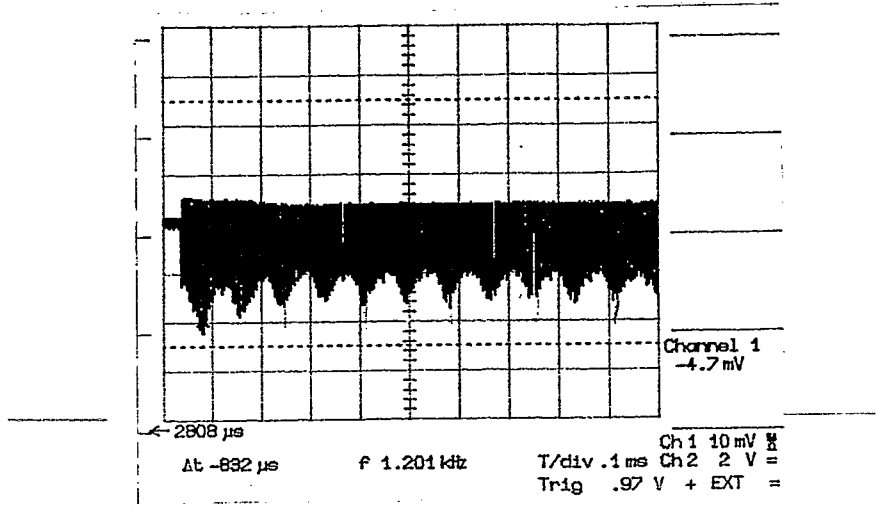


Fig. 11 Synchrotron Oscillations at Injection on Wall Monitor Envelope

On 5/24/89, this technique was used to calibrate the rf system AGS command value and the vector sum signal which appears at the injection console. Table II gives the results.

Table II

Calibration of Total RF Voltage

<u>Total Rf Volts</u> (kV/turn)	<u>AGC Command</u> (computer units)	<u>Vector Sum Magnitude</u> (volts peak-to-peak with 100 Ω termination)
25.7	200	0.0625
147	1000	0.47
235	1515	0.66
253	1615	0.725
263	1715	0.77
276	1815	0.82

A linear fit to the command values gives:

$$\text{Volts/turn} = (0.161 \times \text{command} - 12.0)\text{kV.}$$

Digression into the Transverse Dimensions of Injection

The function of the fast chopper is to eliminate capture losses. It became eminently clear during these studies that a

narrow definition of capture losses, meaning losses caused only because a particle is not injected at the correct rf phase, is not very practical. Longitudinal and transverse effects are strongly interdependent at capture time and a useful injection scheme must respect all mechanisms by which particles can be lost. The study of 5/3/89 concentrated on the transverse dimension (horizontal) and pursued the question what should be done to maximize the probability of survival of every particle injected. We realized that the answer to this question may have little in common with the answer to the question, "what should be done to get the most beam out of the machine given a fixed linac current?". The reason the two answers may be different is that for a high intensity machine space-charge effects dominate and losses are inevitable. One makes tradeoffs in favor of the bottom line, beam out.

In the spirit of a study, however, we decided to concentrate on a low intensity, "non-space-charge" dominated, clean machine, and endeavored to carry out a capture lossless injection. Two basic questions needed to be answered: What beam size (in the horizontal plane) should we create, and at what radius should it be located? In the high intensity world these questions may be profound but in our specialized case, the answers were simple; as small as possible and in the middle of the aperture.

For high intensity, a small beam should be bad because the high charge density aggravates space-charge effects. It would increase the tune spread and cause more particles to travel through stopband resonances. On the other hand, at high intensity there are always some particles at stopbands and if the beam is too big, these are more likely to be quickly lost if there is no "head room" for growth. There may likely be an optimum size and we would like to know how to regulate beam size to exploit such an optimum.

The mechanism for making a small beam size is to eliminate the betatron oscillations that arise as the equilibrium orbit at the stripping foil moves to smaller radius ($\Delta r \approx 14$ mm at fixed momentum) because the main magnet field increases (1.6 out of 250 Gauss) during the ≈ 400 microseconds of the injected pulse.

To understand the procedure followed in the studies to produce a bright beam in horizontal transverse phase space, some description of the AGS injection region and a few definitions must be given. The term "equilibrium orbit" (E.O.) will be used frequently. If a particle circulating around the ring follows exactly the same path on successive turns, that path (which is unique for each given momentum) is its equilibrium orbit. In fact a typical particle will be performing betatron oscillations around its E.O. At any point around the ring, the average of the

particle's position over many passes will also give its E.O. position there. Particles with different momenta (at the same magnetic field) have different E.O.'s (connected by the ring dispersion function).

Figure 12 is a simplified drawing of the injection region. The stripping foil position is fixed during the acceleration cycle (it can be moved on a time scale of minutes) and somewhat restricts the horizontal aperture. A "d.c." $3/2 \lambda$ bump, the "A20 bump", permits the equilibrium orbit to be centered on the aperture remaining. The magnets generating this bump are powered "d.c."; the amplitude of the bump decreases during the acceleration cycle only because the particle rigidity increases. A $1/2 \lambda$ programmable fast bump controls the position of the E.O. relative to the foil during the injection period. The most important function of the fast bump is to quickly move the circulating beam away from the foil once injection is over. Finally, the frame of reference for these bumps is the unbumped orbit. Where this orbit falls in the machine depends on the linac energy (usually held fixed) and the AGS average magnetic field. This field is effectively varied by changing the time at which injection occurs. That is, the injection process is initiated a variable number of microseconds after a variable field trigger (referred to as "peaker") occurs. The "clock" for the field trigger ticks every .02 Gauss. Increasing "peaker" causes all the lines in Figure 12 to move to the inside (up on the figure) except the linac beam and the foil.

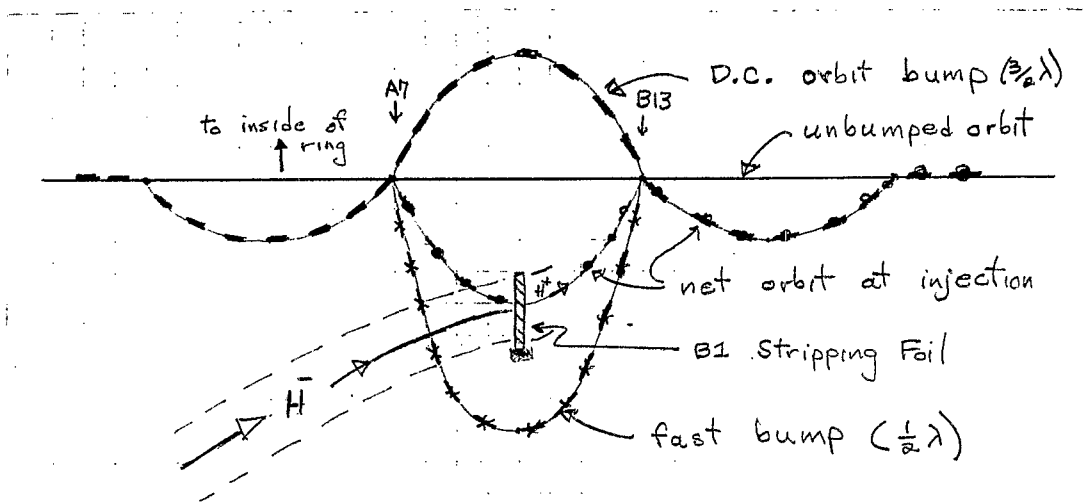


Fig. 12 Simplified Diagram of AGS Injection Region

Let us assume that the bumps are all perfect in the sense of producing no residual orbit distortions around the ring. Further, the foil position is fixed. Then the major horizontal phase space variables are the ring field (injection time) and the amplitudes of the $3/2 \lambda$ and $1/2 \lambda$ bumps (where the latter can be time dependent). Other variables which will be mentioned are the angle and position of the linac beam (controlled by dipoles in the transfer line) and the angle of the ring E.O. at the foil (controlled by low field ring dipoles)

To go with these knobs we have two diagnostic tools; a profile monitor and pick up electrodes (PUEs). The Ionization Profile Monitor (IPM) gives a projection of the beam on a horizontal axis at one point in the ring. Figure 13 gives some IPM data taken with a typical high intensity injection set up except for the setting of peaker, (or magnetic field at injection). The injection field was varied over $(2695 - 2544) = 151$ Gauss clock counts or $(.020/\text{count})$ over 3 Gauss, which corresponds to a motion of the average orbit by about 30 mm, this in addition to the 14 mm sweep during injection. In a) the beam intensity is down [2.9×10^{12} relative to 4.5×10^{12} at c)]; presumably beam is scraping on the outside. In d) the intensity is also somewhat lower than c) so some beam has already hit the inside wall. Beware, the vertical axis is autoscaling. The vertical profiles are essentially invariant to field. The data is taken 150 μs after the end of the injection pulse, integrating for 25 μs .

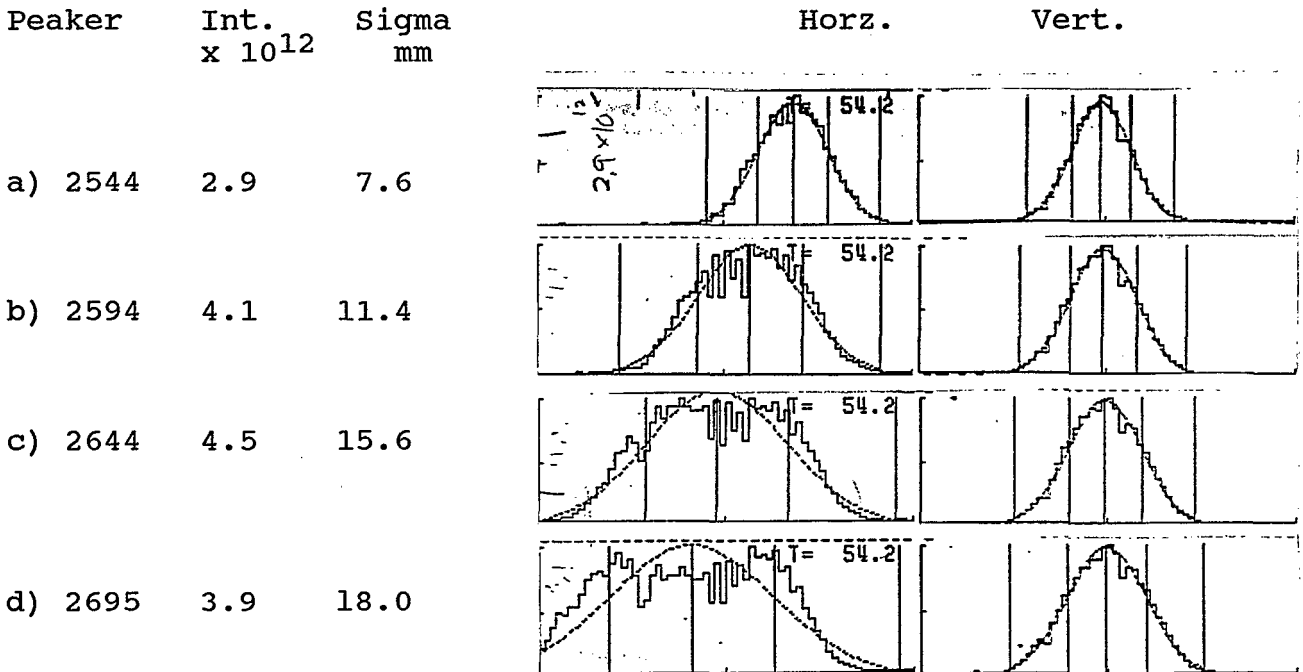
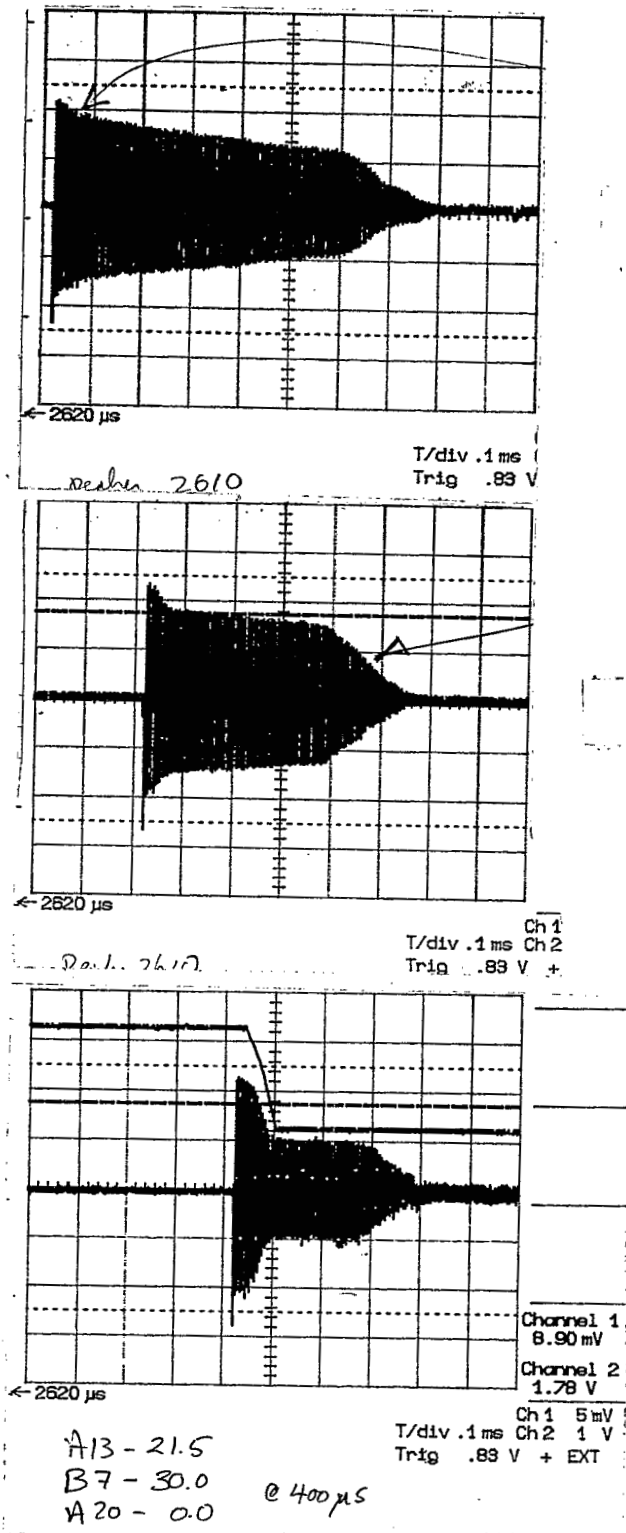
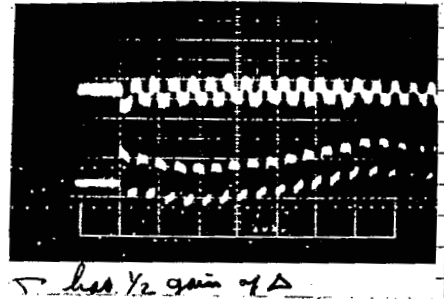


Fig. 13 IPM Scans at Injection Varying Magnetic Field

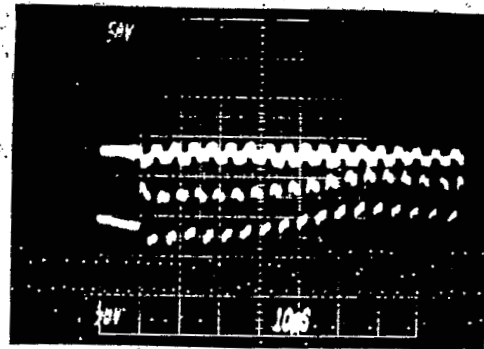
Pairs of ring PUEs give the position of the beam centroid at the PUE location. This information is only available as analog difference signals (scope displays) and responds only to the a.c. component of the beam - which then requires some version of chopping. This diagnostic is quite sensitive to a beam which is not centered on the E.O. since the signal will vary from turn to turn over the full range of the coherent betatron oscillations. The right pictures in Fig. 14 are examples of this diagnostic, the two traces in each photo are the sum of the two plates and the difference for a single half turn of beam seen coming around for many cycles. In this example, the injected beam is well steered so the amplitude of the difference signal is nearly constant turn to turn. Now if the beam from the linac is centered on the E.O. at the foil, the circulating beam in the AGS will have no coherent betatron oscillation. Let us introduce the jargon that such a beam is properly "steered". (The transverse emittance may still grow because the beam emittance may not be matched to the AGS acceptance. This effect will not be discussed further.)



a.



b.



c.

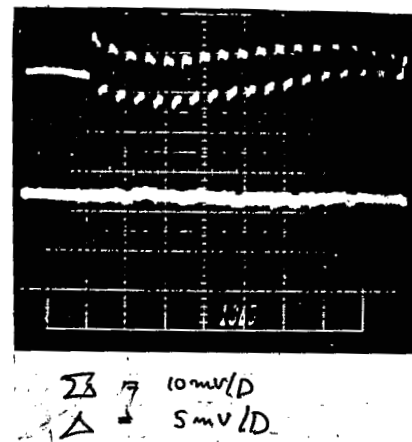


Fig. 14 Spiraling Half Turn Beam (no rf) as seen by the F-20 Wall Monitor (left) and the sum and difference from a horizontal PUE pair (right). (a,b,c): injection time at (start, center, and end) of a hypothetical 400 μ s wide linac pulse.

During the injection interval, the unbumped orbit moves in by ≈ 14 mm. If the fast bump is not time varying to compensate for this motion, an injection which began "steered" will be 14 mm missteered by the end of the 400 μ s pulse. Figure 15 depicts horizontal phase space at the foil and one betatron oscillation wave length away from the foil (and away from the injection bump region). In (a) the first bit of a rather small emittance properly steered beam is seen adiabatically moving inward as the main field ramps during injection. In (b), the last bit of beam (14 mm missteered) is shown on its first pass and then on subsequent passes. Clearly if the bump is not ramped the net emittance grows significantly. Now allow the bump to ramp just enough to hold the E.O. at the injected beam position. Figure 16 (a) and (b) result. The objective then was to ramp the bump to hold the E.O. on the injected beam at the foil.

Operationally this was realized by the following procedure. First the field at the start of the 400 μ s injection pulse was fixed, somewhat arbitrarily, at the normal high intensity value. Then with the fast bump set at a constant value the first 2 μ s of the long pulse was injected into the AGS, and observed with the difference PUEs over many turns. The value of the bump was adjusted to minimize the variation in position over many turns. Since this procedure does not correct an angle error at the foil, some iteration was necessary adjusting the linac angle and the E.O. angle independent of the bump before the situation in Fig. 14a was obtained. The upper trace in the photo shows the beam passing at a fixed position somewhat to the outside. The lower trace gives the sum signal, which confirms that the beam is not being lost. The scope gain for the sum signal was half that for the difference. The PUE calibration is approximately $d = (5 \text{ cm}) [(V_1 - V_2)/(V_1 + V_2)]$ so the orbit is about 13 mm away from the center of the PUE pair. Next a 2 μ s (half turn) from the middle of the long pulse was selected. Now only the bump amplitude was a free parameter. Increasing it slightly yielded the situation in Fig. 14b. Again the position repeats, but is smaller than before - the E.O. has shifted to the inside. Finally, Fig. 14c shows a half turn at the end of the injection pulse, with the bump further increased to null the oscillations. Here the position measured is very near the center of the PUE so the difference trace is essentially a straight line. The function controlling the bump was then adjusted to give the values determined in the above exercise at the appropriate times with a linear interpolation in between. The result is shown in Fig. 17. [Never mind the oscillations early on; injection occurs during the last 400 μ s of the pulse.] The two traces are the currents in the two magnets forming the bump. The currents are not equal because the betatron function differs by a factor of 2 at the two locations and the orbit distortion produced by a given dipole is proportional to the square root of the betatron function.

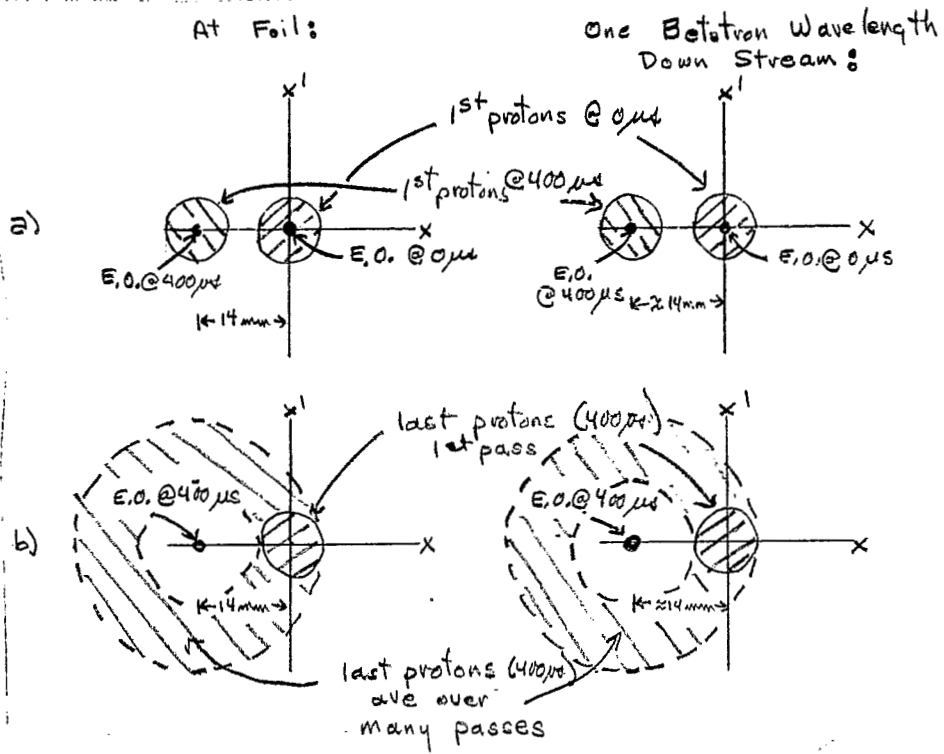


Fig. 15 Horizontal Phase Space Holding Fast Bump Amplitude Constant

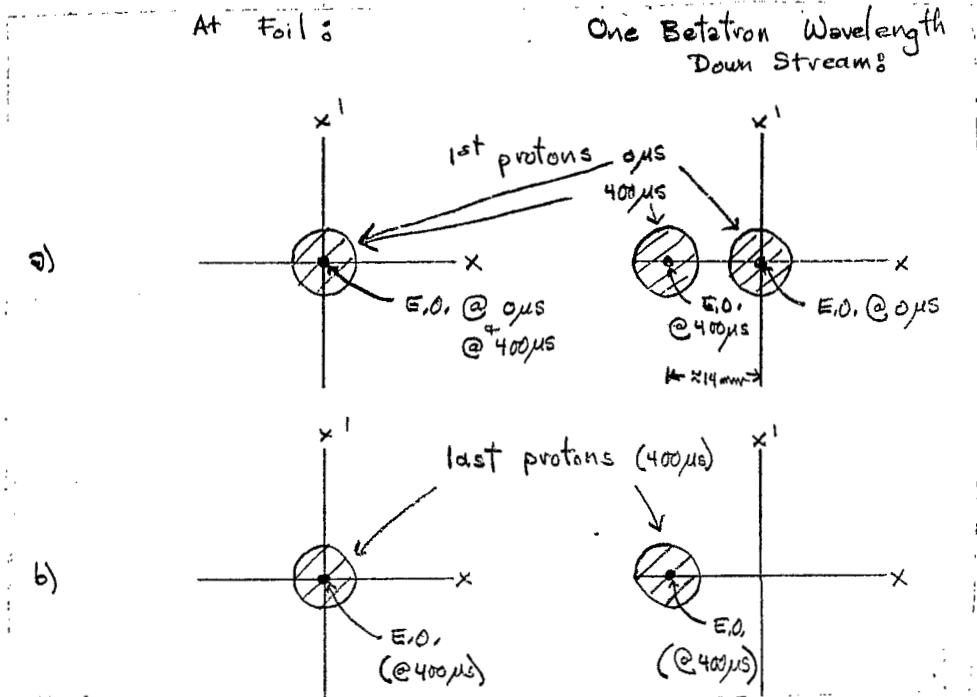


Fig. 16 Horizontal Phase Space Ramping Fast Bump to Hold E.O. Fixed at Foil

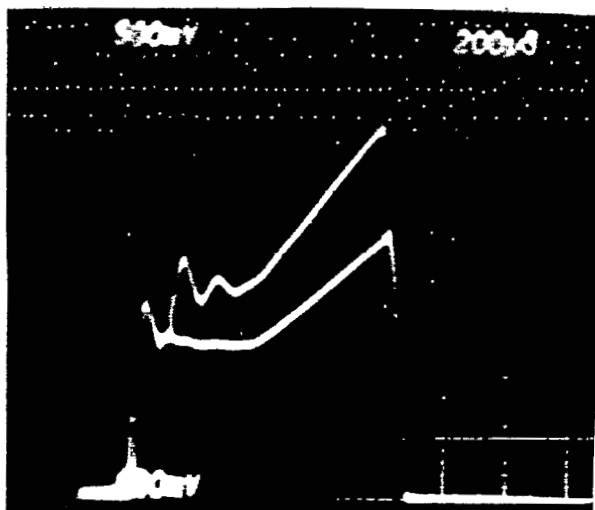


Fig. 17 Currents in Ramped Fast Bump Magnets

The digital scope traces on the left side of Fig. 14 show the output of the F-20 wall monitor for each bump setting. The analogue signals on the right show just the start of the spiraling (left scale $100 \mu\text{s}/\text{cm}$, right $10 \mu\text{s}/\text{cm}$). An apparently unavoidable feature of a properly steered beam was the fast loss ($\approx 50 \mu\text{s}$) at the beginning of the spiral. Moving the linac beam and/or the E.O. and/or the foil itself did not affect this loss qualitatively once a properly steered situation was obtained. In fact, this is an old problem - an apparent outside aperture very near the foil (the effect persists throughout the injection pulse - only near the foil does the beam position remain fixed relative to chamber apertures. The empirical solution to this problem for this study was to move the E.O. somewhat to the inside using the A-20 $3/2 \lambda$ (d.c.) bump superimposed on the previously defined fast bump program. This means the beam is always injected slightly missteered and so the transverse size is slightly increased, but the intensity gain over the full injection pulse was nearly a factor of two. Figure 18a and 18b are transverse phase space sketches demonstrating how a small E.O. shift can dramatically reduce losses (and increase the final emittance).

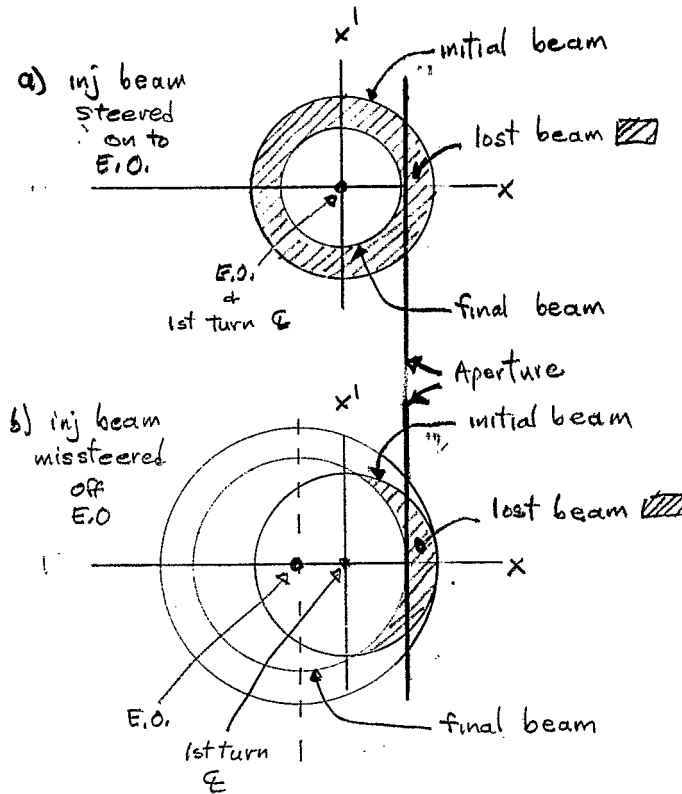


Fig. 18 Horizontal Phase Space Dependence of Beam Loss with Steering

Figure 19 gives IPM data for the beam on the E.O. and with the E.O. shifted inside. (The data is collected over a $125 \mu s$ window just after injection is finished and the fast bump removed). This concludes the transverse phase space discussion but leaves many questions unanswered. Why is there a transverse aperture? Is the transverse emittance measured consistent with the linac emittance and if not, what are the sources of dilution? How do these distributions change as the intensity is increased (linac current increase)?

3-MAY-89 14:36 CH45B.IPD

IPMPL:05/08/86 11-MAY-89 16:23:07

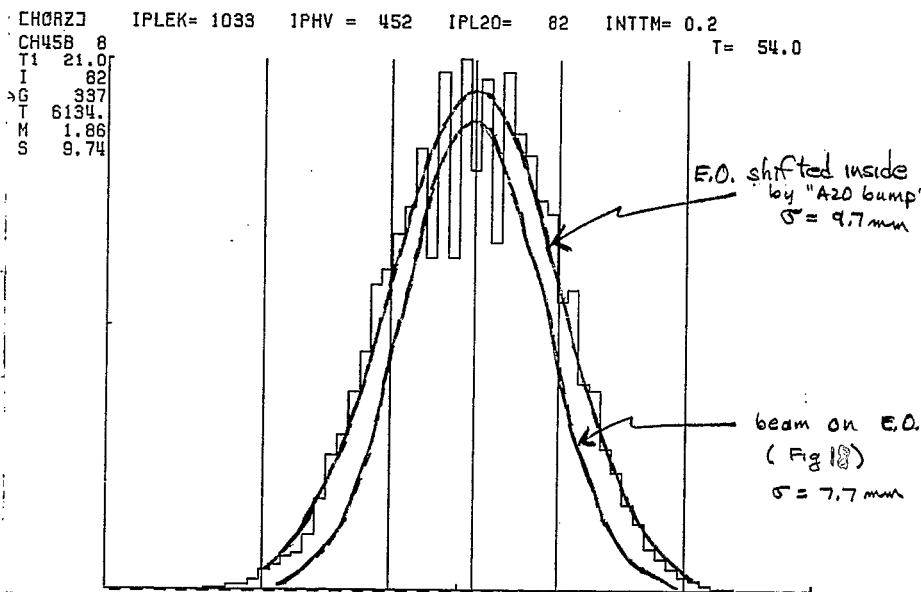
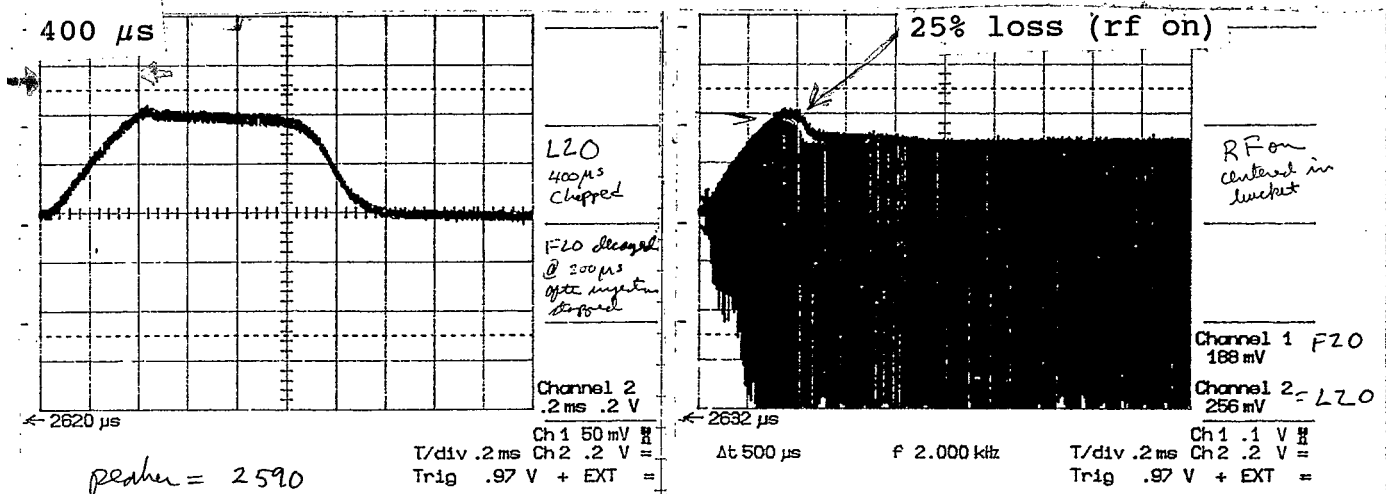


Fig. 19 IPM Scans with Injected Beam Steered and Missteered

A Low Longitudinal Emittance Beam

With this transverse phase space prescription and in particular with the bumps ramped as described above, we injected 100 ns bunches for 400 microseconds. The linac current during each bunch was about 8 mA, giving 5×10^{12} particles. Figure 20a shows the L20 current transformer when the rf was off.



a) Spiraling Beam (rf off) dc monitor (L20) b) Accelerating Beam dc & ac (F20) monitor

Fig. 20 Current of Beam in AGS

About 2.5×10^{12} particles spiral for 700 microseconds. With the rf turned on at 230 keV turn peak voltage, and the frequency slope at 33 kHz/ms (to create a moving bucket so that $dR/dt = 0$), the beam was injected at the center of the bucket. The frequency of the center of the bucket was known from the measurement of the revolution frequency with a single bunch. The phase of the center of the bucket was found empirically. Figure 21a shows the characteristic mountain range pattern for a single turn at the center of the bucket. For fine tuning, this pattern reveals misadjustments of phase and frequency in different ways. In Fig. 21b, the phase is incorrect, and the base wiggles; in Fig. 21c, the frequency is wrong the peaks wiggle.

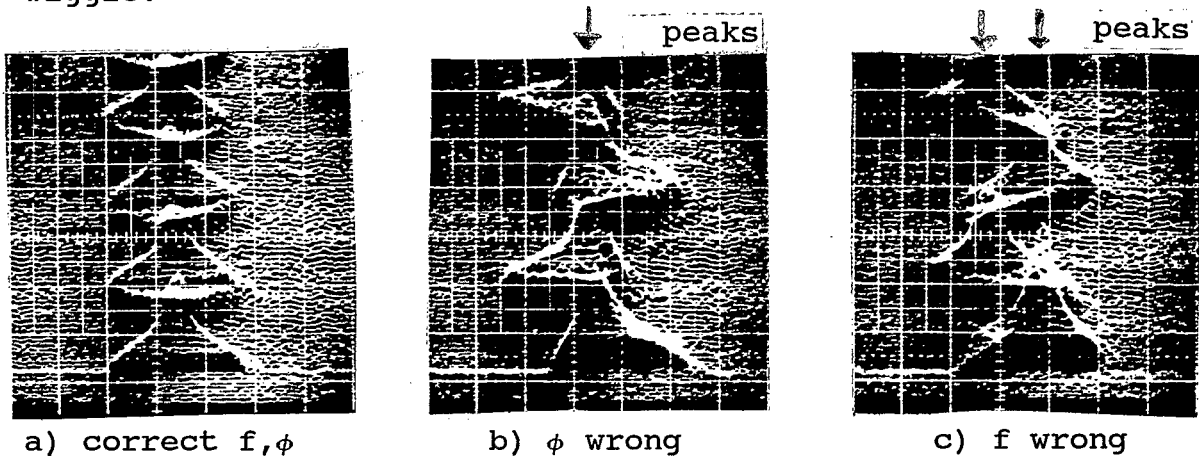


Fig. 21 Wall Monitor Mountain Range at Injection with Variation of Phase and Frequency of Bucket Relative to Bunch

A 25% beam loss occurred when the rf was turned on. This can be seen in Fig. 20b where the F20 wall current monitor was added to the L-20 current transformer display of Fig. 20a.

The F20 signal is negative going so that the top of this display is the base line. For an a.c. coupled pick-up at fixed frequency, the base line is directly proportional to the a.c. component of the beam current. The scope scale factors have been adjusted so that the vertical axis has the same calibration for both the L20 current transformer and the F20 wall monitor. A crucial difference between the two is that the L20 signal has very low frequency response and hence is sensitive to all the beam in the machine, whereas, the F20 signal is sensitive only to the ac component of the beam current. One can see the 25% loss in both traces. This loss is most likely caused by the synchrotron motion of the beam in the bucket causing it to make radial excursions outside the horizontal aperture. The excursions are ± 6 mm on the average, that is, for the average dispersion. There is an indication in Fig. 20b that the ac component of the beam is lost 20 microseconds before this 25% is finally gone from the

machine. One possible explanation for this is that these particles traverse some "foil" of the appropriate thickness that their energy changes enough immediately to knock them out of the bucket but not enough to kick them completely out of the machine.

The longitudinal emittance of this beam was measured at four momenta as the beam was accelerated to full energy and extracted. Plots of the wall current monitor signal at 0.86, 3.68, 9.63, and 15.4 GeV/c are shown in Figs. 22a to 22d. The plots were taken with the TEK2467 scope and the digitizing camera system. The horizontal scale in all plots is 1.17 microseconds per full scale. After the study, when the machine was returned to normal operation, similar plots were taken. They are shown in Fig. 23a to 23d. The plot in Fig. 23a is at 1.15 GeV/c momentum. The data and results of the longitudinal emittance measurements are compiled in Table III, and the results are plotted in Fig. 24.

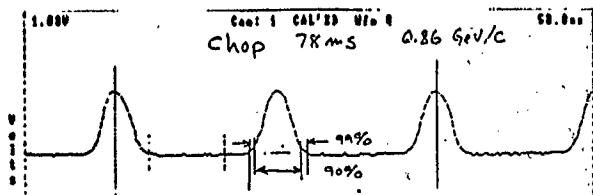
Results are quoted for "99%" and "90%" of the beam. The definitions for these cuts are indicated by markers on the data plots. From Fig. 24, one can see that by chopping an emittance of approximately 1/3 the normal 0.9 eV sec per bunch value was created and essentially preserved throughout the cycle. In normal operation, when the intensity is ten times greater, the emittance grows by a large factor while crossing transition. Also plotted in Fig. 24 is the area of the moving bucket. One can see that the high intensity beam fills the bucket after transition.

A Practical Injection Scheme

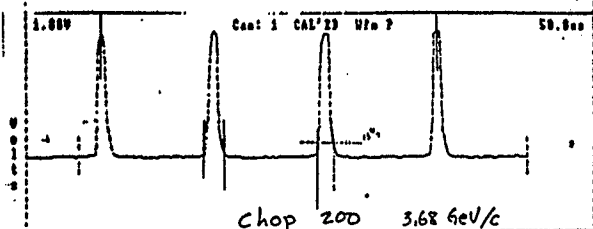
Figure 25 is the same type of display as Fig. 20b except that it is from normal high intensity running without chopped beam. Since the incoming beam is continuous, it has no a.c. component until it is bunched by the rf system, and not all the beam is bunched. The most significant feature of the figure is the 35% loss in intensity in both the L20 current transformer and the F20 wall monitor signal that takes place over about 1.2 ms after injection is complete. For a practical injection scheme, we require that not only is all the beam within the rf bucket but also that most of the beam survive this critical milliseconds after injection.

The small beam created by ramping the bumps does survive well, as seen in Fig. 20a. The loss seen in Fig. 20b, when the rf is on, is caused by two effects, both of which can be eliminated by the proper choice of the rf system parameters. One effect is that the moving bucket accelerates particles and holds the radius of the first injected particles fixed while the radius

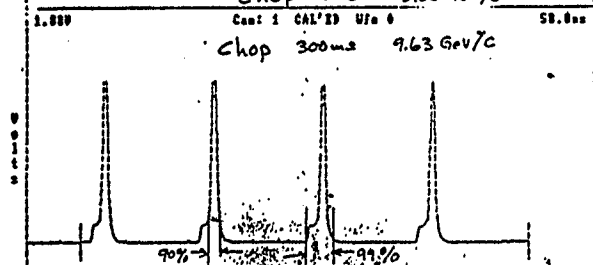
a. (.86 GeV/c)



b. (3.68 GeV/c)



c. (9.63 GeV/c)



d. (15.4 GeV/c)

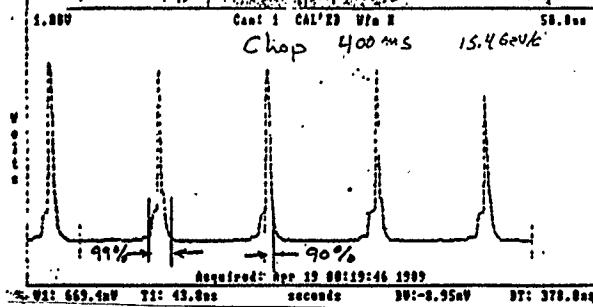
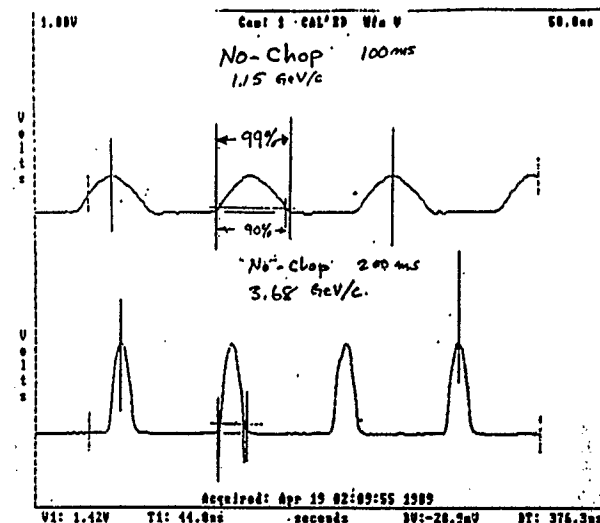
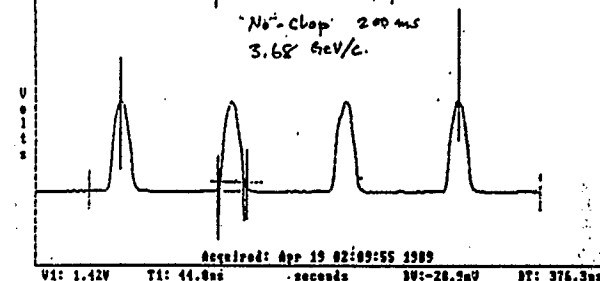


Fig. 22 Bunch Length Chopped Beam

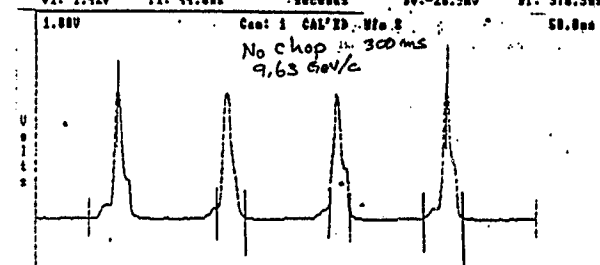
a. (1.15 GeV/c)



b. (3.68 GeV/c)



c. (9.63 GeV/c)



d. (15.4 GeV/c)

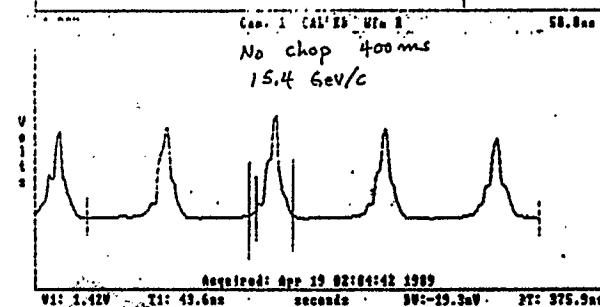


Fig. 23 Bunch Length Unchopped Beam

Table III
 Longitudinal Emittance During Acceleration
 $V_{rf} = 230 \text{ kV/Turn}$

Time	CP	B	ϕ_s	Bucket		Width					
				ϵ	f^{-1}	90%	99%	90%	99%		
T_0, ms	GeV	T/S	Deg.	n	ns	ns	Deg.	ns	Deg.	ev.s	ev.s
78	0.86	0.45	7.7	1.16	330	93	102	118	128	.23	.35
200	3.68	2.2	40.5	1.84	231	31	48	43	68	.27	.51
Chop 300	9.63	2.3	136.5	8.2	225	25	40	56	90	.94	4.4
400	15.4	2.2	140.2	8.3	223	19	30	46	75	.45	2.7
No	100	1.15	0.45	7.7	1.47	288	137	171	149	.75	.87
200	3.68	2.2	40.5	1.84	231	50	77	62	96	.65	.98
Chop 300	9.63	2.3	136.5	8.2	225	43	70	81	130	2.7	7.7
400	15.4	2.2	140.2	8.3	223	75	120	87	140	6.2	7.7

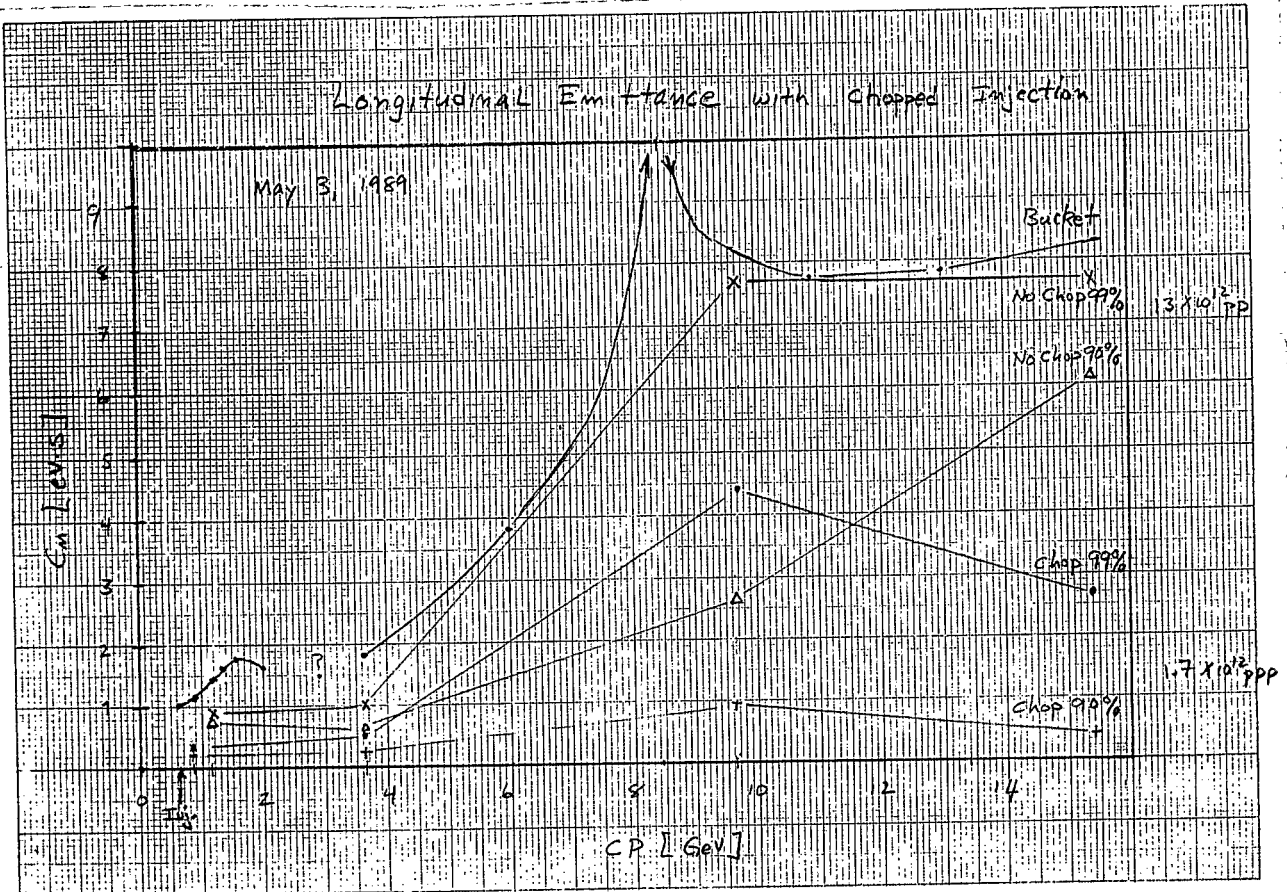


Fig. 24 Longitudinal Emittance vs Energy

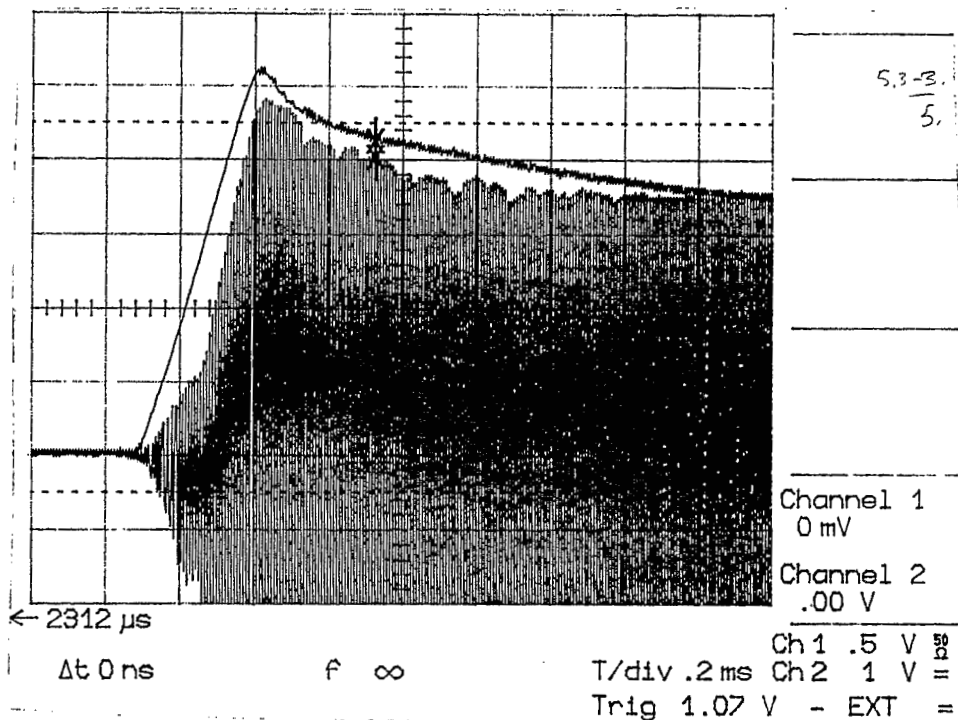


Fig. 25 Beam Intensity vs Time Near Injection L-20 (dc) and F-20 (ac) High Intensity Set Up

of the particles injected later is reduced by the increasing main magnet field. This partially undoes the effect of ramping the bumps and leads to a larger size beam, with less "head room". This need not happen with rf on, if only the frequency slope is set to 0.7 kHz/ms, which makes a stationary bucket and does not accelerate the early injected particles. The other effect is the synchrotron motion driving radial excursions into some horizontal aperture. This effect can be nearly eliminated by injecting into a very low voltage rf bucket, so that the radial excursions are small. In fact, knowing the linac beam energy spread, one can choose the rf voltage so that the beam is nearly matched to the bucket and then very little bunch shape oscillation takes place.

This injection scheme was modeled on the computer (Private Communication: Joseph Kats) and the results of the simulation are shown in Fig. 26. On 5/24/89, this scheme was implemented in a study with the fast chopper. The transition from the low voltage stationary bucket to the high voltage moving bucket is somewhat smooth and the programs for frequency versus time and voltage versus time were taken from the simulation.

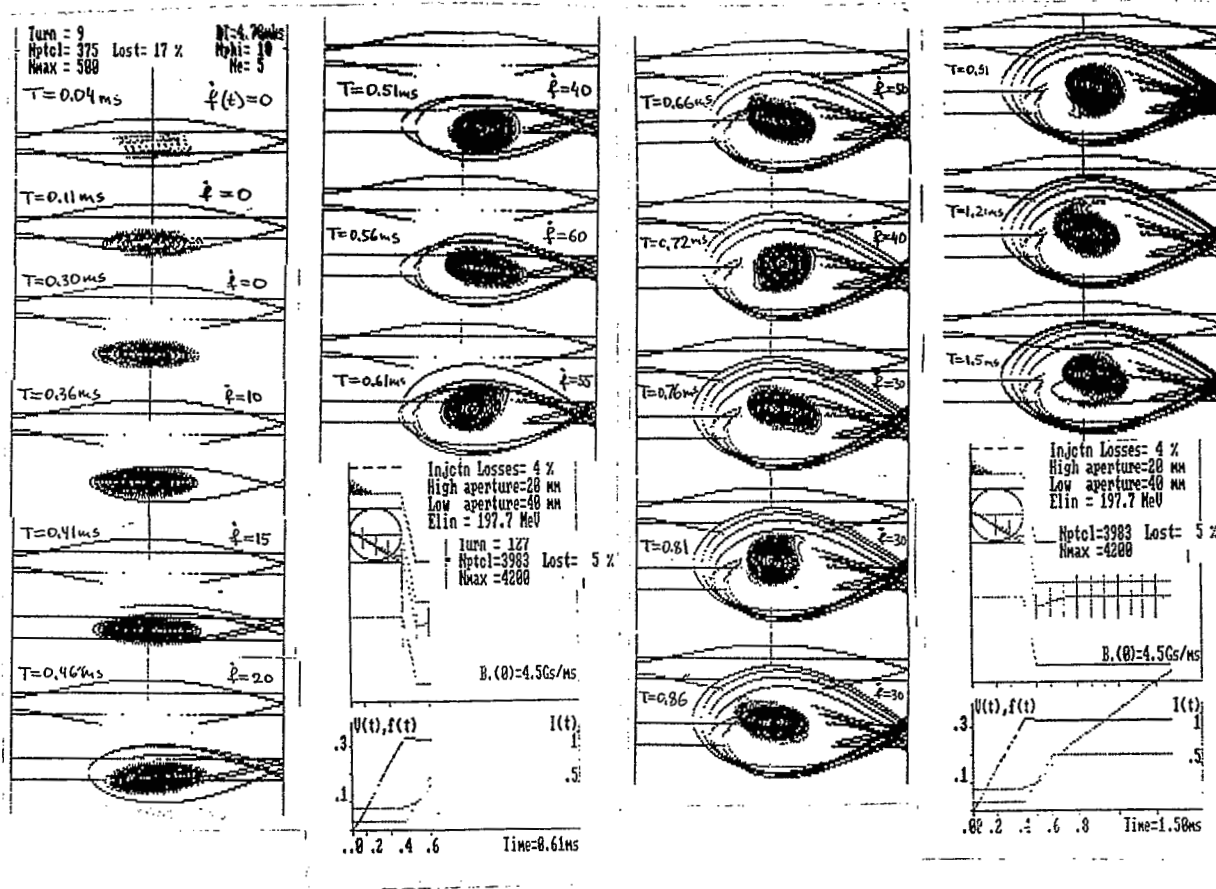


Fig. 26 Computer Simulation of "Low Voltage, Ramping B, Stationary Bucket" Injection Scheme

Frequency versus time is shown in Fig. 27 from the HP5371 frequency analyzer. The frequency was obtained by putting a PDP10-controlled function generator through a lowpass filter and then into the FM input of a HP8656 rf synthesizer and using the synthesizer output as the starting oscillator for the rf system. In the figure, the horizontal axis is zero to 3.0 ms full scale and the beam injection ends at the marker "X". The vertical axis (frequency) spans 2.5120 MHz to 2.6000 MHz. The voltage program is shown in Fig. 28. The gap voltage is raised form 26 keV/turn in 400 microseconds, starting after injection is complete.

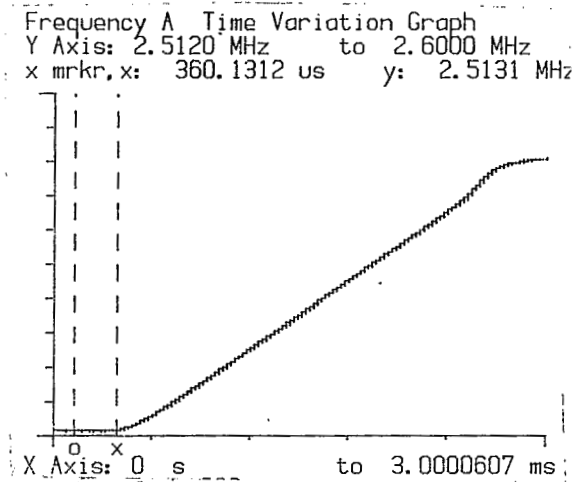


Fig. 27 RF Frequency vs Time during Injection Capture

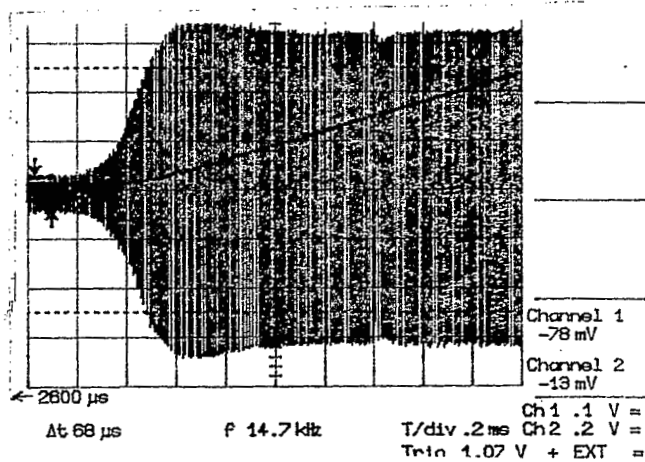


Fig. 28 Voltage Program (RF Vector Sum Envelope) during Injection/Capture

The scheme was first tried with 100 ns bunches injected. The result is shown in Fig. 29 where L20 and F20 are both displayed. Clearly, all the beam is in the bucket and the only loss is about 10% loss that takes place for about 100 microseconds after the end of injection. This 10% loss was not predicted by the simulation calculation.

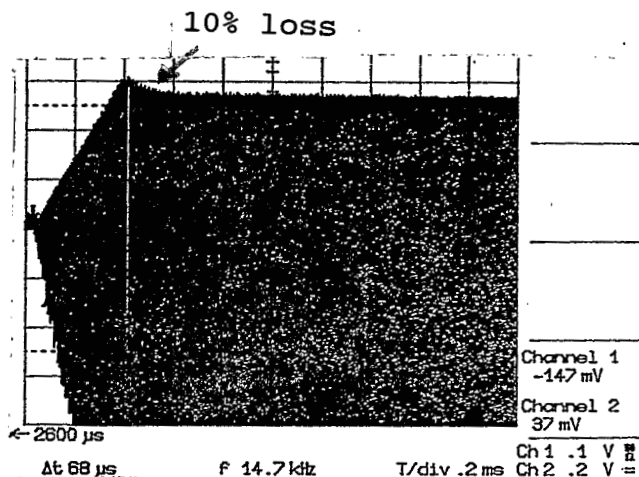


Fig. 29 Beam Current (F20 + L20) For Superimposed "Low Voltage Stationary Bucket" Capture Scheme

It was found, by some trial and error, that if the fast injection bumps were turned off slightly early, about 40 microseconds before the end of injection, the 10% loss was reduced to essentially zero. This fact is evidenced in Fig. 30a. Also shown in Figs. 30c and 30d are mountain range pictures of the bunch forming as the beam is stacked in and the final bunch as it begins to be accelerated. A photograph of the scalars at the injection console in Fig. 30b shows that 5.2×10^{12} particles came from the linac, 3.4×10^{12} particles were injected, and 3.1×10^{12} particles survived out to 3 ms.

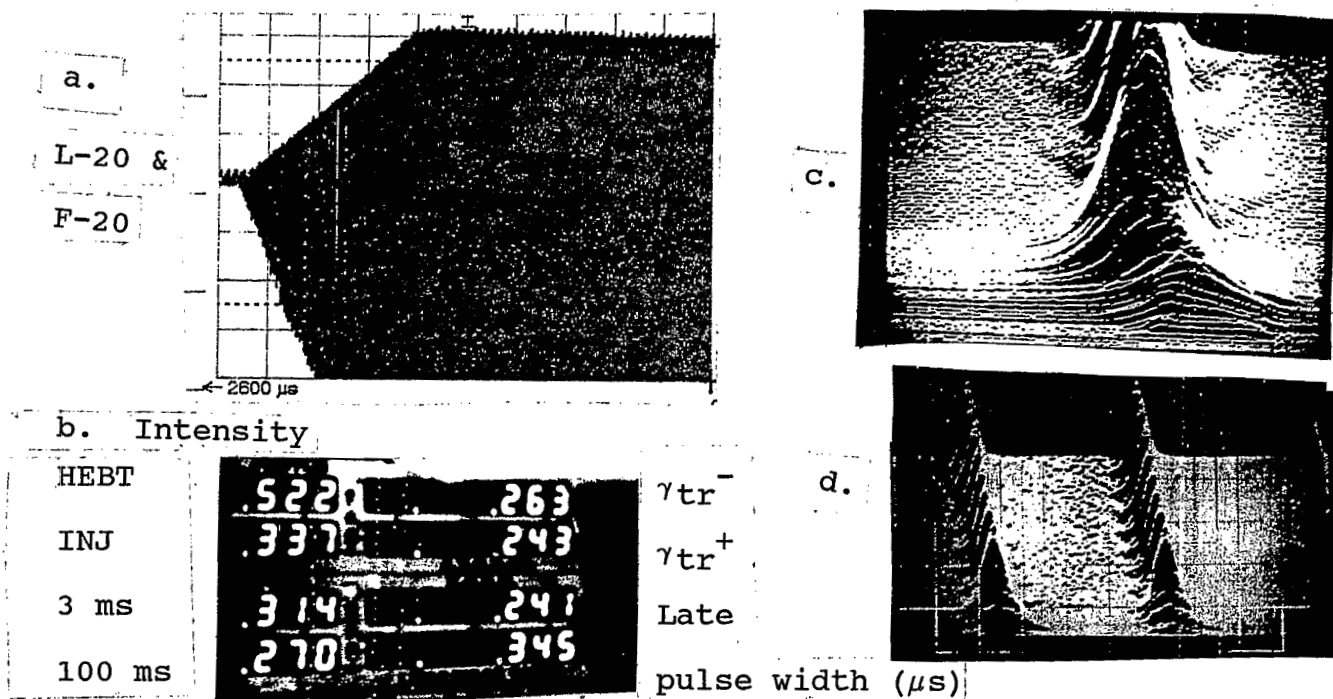


Fig. 30 "Lossless" Capture at 3×10^{12} Protons

The bunch width was then increased from 100 to 300 ns. The result is shown in Fig. 31a. The intensity here was nontrivial and yet capture losses, in the broad sense of the term, were low. The scalars in Fig. 31b show that 2.5×10^{13} particles came from the linac, 1.5×10^{13} were injected, and 1.3×10^{13} survived out to 3 ms. Figure 31d is a mountain range picture for this nearly full-bucket situation. Figure 31c shows the L20 signal (top trace), the radial position (next one down), and the two bump currents. One can see that the bumps were switched off before the end of injection. It should be noted that when the bunch width was increased by a factor of three, the total number of particles from the linac increased by a factor of five. This nonlinear response is a manifestation of the space-charge effect of the chopper mentioned in section one.

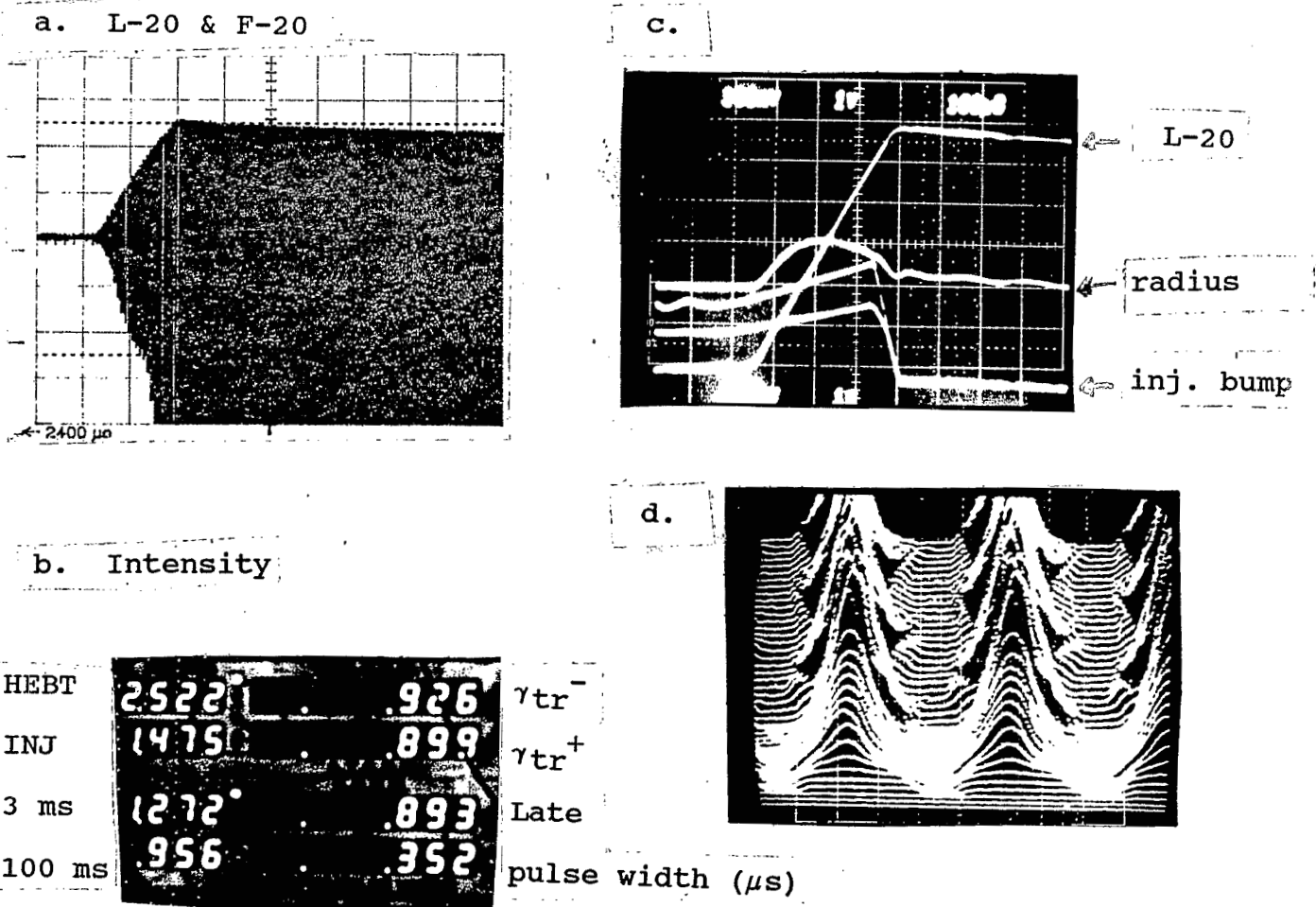


Fig. 31 Capture Setup with 1×10^{13} Protons

Conclusion

An essentially "capture lossless" injection scheme has been carried out using the fast chopper. At intensities approaching normal operating values, the capture losses are still lower than what heretofore has been achieved. The most surprising result of these studies is that a scheme that was intended to be effective only at low intensities, because it involved making a small beam size, turned out to give low capture and early acceleration losses, even at 1.3×10^{13} particles captured. Perhaps the beam was redistributing itself in transverse phase space without the help of a large initial "betatron space" distribution, perhaps not. Transverse measurements in this high intensity regime are needed to clarify the situation.

Acknowledgements

We would like to thank several people for their essential help in bringing the fast chopper into operation. The linac staff, in particular, Brian Briscoe and Vincent LoDestro built the hardware necessary to integrate the fast chopper into normal linac operations. They also willingly accepted the new, and somewhat unconventional, device into their list of responsibilities. In the computer controls group, Joe Skelly, Brian Oerter, and Vincent Wong did the behind-the-scenes work that made using the fast chopper from the main control room possible. Joe Kats contributed a key ingredient to this work when he explained the concept of the stationary bucket in the rising magnetic field. He also performed several computer simulation calculations of rf capture. Interfacing to the low-level rf system of the AGS would not have been possible without the advice and support of Edward Gill. Alex Zaltsman spoke for the high-level rf. In particular the work his group has done over the past year on the cavity tuning loop permitted the low voltage operation at injection. The state-of-the-art data taking facilities in the main control room were the handy work of Willem van Asselt who collaborated in the studies runs.